Molecular Orientational Dynamics in K_3C_{60} Probed by Two-Dimensional Nuclear Magnetic Resonance

S. E. Barrett and R. Tycko

AT&T Bell Laboratories, 600 Mountain Avenue, Murray Hill, New Jersey 07974

(Received 10 September 1992)

We characterize the orientational dynamics of C_{60}^{3-} anions in K_3C_{60}, using two-dimensional NMR exchange spectroscopy. We find an activated temperature dependence for the reorientation rate between 195 and 220 K, with $E_a = 460 \pm 60$ meV. Molecular reorientation proceeds via small ($< 44°$) rotational jumps, implying that K_3C_{60} is more highly orientationally disordered than previously proposed.

PACS numbers: 61.50.−f, 33.25.−j, 74.70.Ya, 76.60.−k

Molecular orientational dynamics and static orientational disorder in solid C_{60} have been shown to be important because of their relation to the orientational order-disorder transition [1–3] and their influence on sound velocity [4], thermal conductivity [5], and dielectric response [6] measurements. In addition, measurements of orientational dynamics provide a test for models of intermolecular interactions [7]. In alkali fullerides A_xC_{60}, orientational dynamics and orientational ordering of C_{60}^{x-} anions may also be expected to influence the low-temperature electronic properties [8]. In this Letter, we report a quantitative study of molecular orientational dynamics in K_3C_{60} (a superconductor with $T_c = 19$ K) [9], using one- and two-dimensional (1D and 2D) ^{13}C NMR. We find that the energy barrier for large-amplitude molecular reorientations is 460 ± 60 meV (1.8 times larger than in the $T < 260$ K "ordered" phase of C_{60}) [3–6] and that large-amplitude reorientations proceed via small-angle rotational jumps. The latter result implies a structure for K_3C_{60} with considerably more disorder than previously proposed [10].

Figures 1(a)–1(c) show 1D ^{13}C NMR spectra of K_3C_{60} at several temperatures. The 35-mg powder sample was prepared as described previously [9,11] and sealed in a pyrex tube with 1 atm of helium gas. The spectra were acquired at 100.48 MHz (9.39 T field) using a Chemagnetics CMX spectrometer and home-built low-temperature probes. At 200 K [Fig. 1(c)], an inhomogeneously broadened line is observed, with a linewidth $\Delta\nu \approx 10$ kHz and a shape which is not characteristic of a single magnetic (Knight plus chemical) shift anisotropy tensor [12]. This line shape can be approximated as the superposition of four shift anisotropy powder patterns [principal values $(\delta_{11},\delta_{22},\delta_{33}) = (218.5, 179.6, 133.0)$, (234.1, 179.6, 125.2), (257.4, 187.4, 117.6), (280.7, 175.0, 94.1), in ppm relative to tetramethylsilane] as shown in Fig. 1(d). The Knight shift contribution to the K_3C_{60} line shape may explain the complicated superposition, which differs from the well-defined chemical shift anisotropy powder pattern in C_{60} [3]. In K_3C_{60}, the ^{13}C NMR frequency of a particular nucleus depends on the molecular orientation relative to the crystal axes as well as the molecular orientation relative to the external magnetic field. A small peak at 143 ppm, attributed to $< 7\%$ residual pure C_{60}, is also observed in the spectrum below 260 K, where the orientational ordering transition in C_{60} causes the ^{13}C spin-lattice relaxation time T_1 to decrease abruptly [3].

Figure 1(a) shows that a single motionally narrowed line (0.9 kHz wide at 330 K) is observed in the 1D spectrum at high temperatures, since isotropic reorientations on a time scale $\tau_R \ll 1/\Delta\nu$ average out the anisotropy of the NMR frequency. The onset of motional narrowing occurs when $\tau_R \Delta\nu \sim 1$, indicating that $\tau_R \ll 100$ μs in K_3C_{60} above 300 K.

In pure C_{60}, the temperature dependence of τ_R was determined quantitatively from ^{13}C NMR T_1 measurements [3]. In K_3C_{60}, the dominant nuclear spin-lattice

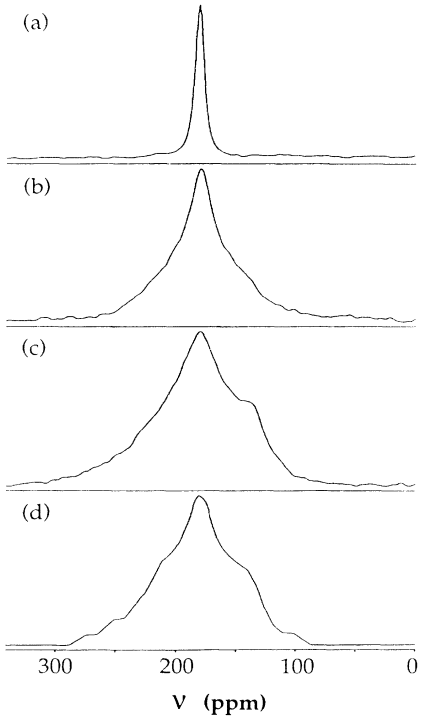

FIG. 1. 1D ^{13}C NMR spectra of K_3C_{60} at (a) $T = 330$ K, (b) 260 K, (c) 200 K. (d) A simulation of the line shape in (c).

relaxation mechanism is provided by hyperfine couplings to conduction electrons [12,13], rather than by coupling to molecular reorientations through the chemical shift anisotropy as in pure C_{60} [3]. Therefore, T_1 measurements do not probe orientational dynamics in K_3C_{60}. Instead, we use 2D NMR exchange spectroscopy [14], as used by others to study orientational dynamics in solid polymers [15], for example. 2D exchange spectra probe dynamics on the time scale $1/\Delta\nu < \tau_R \leq T_1$, which is satisfied for $195 < T < 220$ K in K_3C_{60}. We acquire 2D exchange data using the pulse sequence $90_{\phi_1} - t_1 - 90_{\phi_2} - \tau_e - 90_{\phi_3} - t_d - 180_{\phi_4} - t_d - t_2$, with phase cycling of ϕ_1, ϕ_2, ϕ_3, and ϕ_4 to eliminate artifacts. In each data set, the exchange period τ_e is kept fixed, t_1 is incremented from 0.5 to 1600.5 μs, and NMR signals are digitized during the detection period t_2 for each t_1 value (the final two pulses produce spin echoes; $t_d = 50$ μs). Fourier transformation of the signals $S(t_1,t_2;\tau_e)$ with respect to t_1 and t_2 yields a 2D spectrum $F(\nu_1,\nu_2;\tau_e)$ which reveals the correlations of NMR frequencies before (ν_1) and after (ν_2) the exchange period τ_e.

Representative 2D spectra for $T = 210$ and 220 K, displayed as contour plots, are shown in Figs. 2(a), 2(d), and 2(g) and 2(b), 2(e), and 2(f). The data at the two temperatures are quite similar, except for the different τ_e values. For $\tau_e \ll \tau_R$, the molecular orientations and hence the NMR frequencies do not change significantly during τ_e. The spectral intensity then lies along the diagonal ($\nu_1 = \nu_2$) of the 2D plot [see Figs. 2(a) and 2(b)]. For $\tau_e \geq \tau_R$, large-amplitude reorientations, and hence large changes in the NMR frequencies, are likely during τ_e. Significant off-diagonal intensity then develops [see Figs. 2(d) and 2(e)]. The fact that off-diagonal intensity develops at shorter values of τ_e at 220 K than at 210 K indicates that reorientation is more rapid at the higher temperature, as expected.

We extract kinetic parameters by fitting the experimental 2D data to simulated 2D spectra, based on a rotational diffusion model and using the line shape in Fig. 1(d). To simulate the development of the 2D spectrum, we represent τ_e by N time steps. In each step, we apply a 5° rotation about a randomly chosen axis to each shift tensor (to approximate isotropic rotational diffusion). Simulated, powder-averaged 2D spectra $F_s(\nu_1,\nu_2;N)$ are then calculated for each N by summing the contributions to the spectra from many initial shift tensor orientations

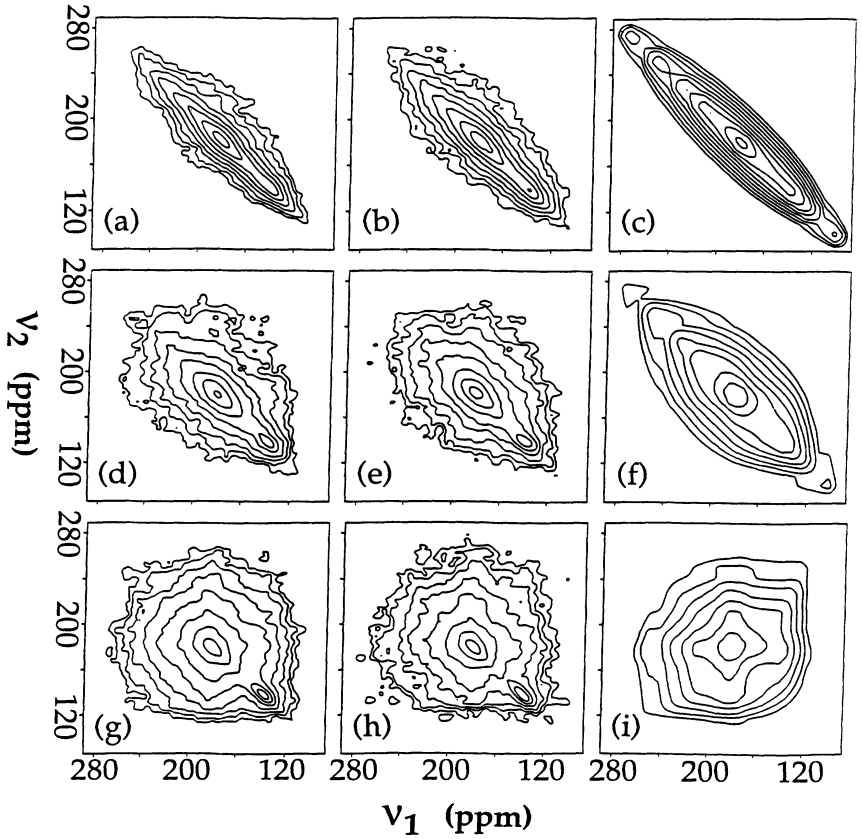

FIG. 2. 2D ^{13}C NMR exchange spectra of K_3C_{60} for the following temperatures and exchange times τ_e: (a) 210 K, 3 ms; (b) 220 K, 1 ms; (d) 210 K, 22 ms; (e) 220 K, 7 ms; (g) 210 K, 200 ms; (h) 220 K, 60 ms. Simulated exchange spectra assuming isotropic rotational diffusion of C_{60}^{3-} anions for (c) 10, (f) 68, and (i) 578 time steps.

and many runs. Representative 2D simulations are shown in Figs. 2(c), 2(f), and 2(g). The simulations reproduce the qualitative features of the experiments, but differ in certain details due to the necessarily approximate nature of the line shape used in the simulations. We then perform a least-squares fit of each experimental 2D spectrum to the simulations [over a restricted region of comparison in the (ν_1,ν_2) plane to avoid the residual C_{60} peak in the experimental data], yielding an optimal number of time steps for each τ_e and temperature, $N_{\rm opt}(\tau_e,T)$.

Figure 3(a) shows a plot of $N_{\rm opt}$ vs τ_e for $T=220$ K. For short τ_e (circles), the points can be fitted by a straight line through the origin with slope $\Delta N_{\rm opt}/\Delta\tau_e$. For long τ_e (triangles), the points systematically deviate from this line. This deviation is attributed to discrepancies between the 1D spectrum [Fig. 1(c)] and the approximate line shape used in simulations [Fig. 1(d)]. These discrepancies are most important when comparing long τ_e 2D spectra [Figs. 2(g) and 2(h)] with large N simulations [Fig. 2(i)]. We therefore exclude the long τ_e points from further analysis. The rotational diffusion constant is then given by $D_{\rm rot}=1.27(\Delta N_{\rm opt}/\Delta\tau_e)10^{-3}$ $(=1/6\tau_R$, where τ_R is the orientational correlation time for second rank tensors) [16]. Figure 3(b) shows an Arrhenius plot of $D_{\rm rot}$ vs $1/k_BT$. A weighted least-squares fit by the form $D_{\rm rot}=A\exp(-E_a/k_BT)$ yields the best-fit values $A=10^{11.6\pm1.4}$ rad^2/sec and $E_a=460\pm60$ meV. These parameters imply $\tau_R=100$ μs at 276 K, consistent with the 1D motional narrowing result. Our value for E_a is in agreement with a rough estimate ($E_a\sim500$ meV) from inelastic neutron scattering measurements [17]. The value we obtain for E_a in K_3C_{60} is closer to the value observed in the "orientationally ordered," low-temperature phase of pure C_{60} ($E_a\approx250$ meV) [3–6] than to that found in the disordered, high-temperature phase of C_{60} ($E_a\approx42$ meV) [3]. This suggests that the nature of the structure and dynamics of K_3C_{60} around 200 K is more closely related to that in orientationally ordered pure C_{60}. The factor of 1.8 difference between E_a in these two materials may be due to steric hindrance of molecular reorientations by K^+ in tetrahedral interstitial sites in K_3C_{60} and to Coulombic interactions among C_{60}^{3-} anions and K^+.

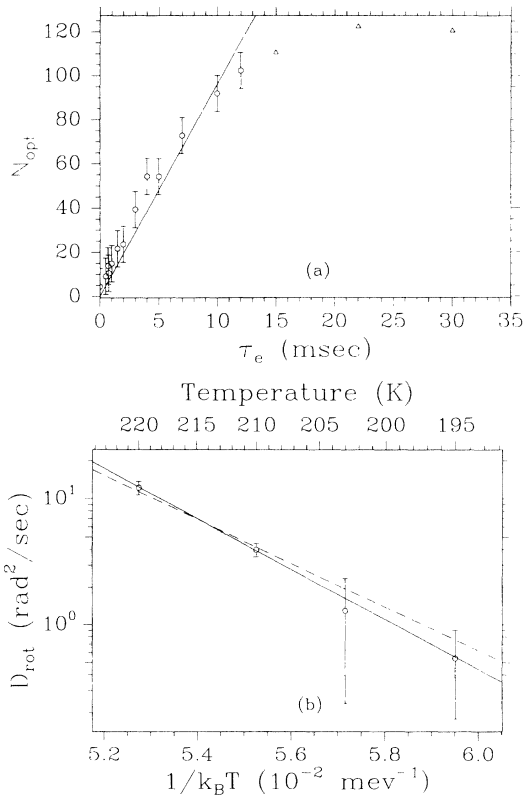

FIG. 3. (a) Optimal number of time steps $N_{\rm opt}$ for each τ_e at $T=220$ K obtained by a least-squares fit of experimental 2D spectra to simulations, as in Fig. 2. The short τ_e points (circles) are fitted by a straight line with slope $\Delta N_{\rm opt}/\Delta\tau_e=9.6\pm1.2$ ms^{-1}. (b) Temperature dependence of the rotational diffusion constant $D_{\rm rot}=1.27(\Delta N_{\rm opt}/\Delta\tau_e)10^3$. A weighted least-squares fit by the form $D_{\rm rot}=A\,e^{-(E_a/k_BT)}$ is shown (solid line), along with ±1 standard deviation limits (dashed and dotted lines).

Further microscopic details of the molecular reorientation process in K_3C_{60} can be elucidated by comparing our experimental 2D spectra with simulations for alternative models of the dynamics. The first model assumes a fully orientationally ordered structure, implying that large-amplitude molecular reorientations can only occur via $(360/n)°$ jumps about n-fold symmetry axes ($n=2,3,5$). Figures 4(a)–4(c) show simulated 2D spectra for the $n=5$ case, assuming equal rates for all possible 72° jumps. The simulations for the $n=2$ and $n=3$ cases yield nearly indistinguishable results. These simulations disagree qualitatively with the experimental data in two respects. First, the long τ_e simulations [e.g., Fig. 4(c)] show a pronounced ridge along the diagonal, absent from Figs. 2(g)–2(i), that results from the significant probability that a given molecule will have the same orientation before and after τ_e in an orientationally ordered structure. Second, the large angle of each rotational jump (at least 72°) permits large changes in the NMR frequencies in a single jump, causing the simulated spectra at intermediate τ_e [Fig. 4(b)] to resemble superpositions of short τ_e [Fig. 4(a)] and long τ_e simulations. As τ_e is increased from zero, spectral intensity far from the diagonal appears quickly in these simulations, in contrast to the gradual diffusion of spectral intensity away from the diagonal in the experimental spectra [Figs. 2(d) and 2(e)] and rotational diffusion simulations [Fig. 2(f)].

Based on x-ray diffraction, an $Fm\bar{3}m$ crystal structure has been proposed for K_3C_{60}, in which each C_{60}^{3-} may adopt with equal probability either of two inequivalent orientations, related by 90° rotations about the twofold axes lying along the ⟨100⟩ directions [10]. In a model of the orientational dynamics that is consistent with this

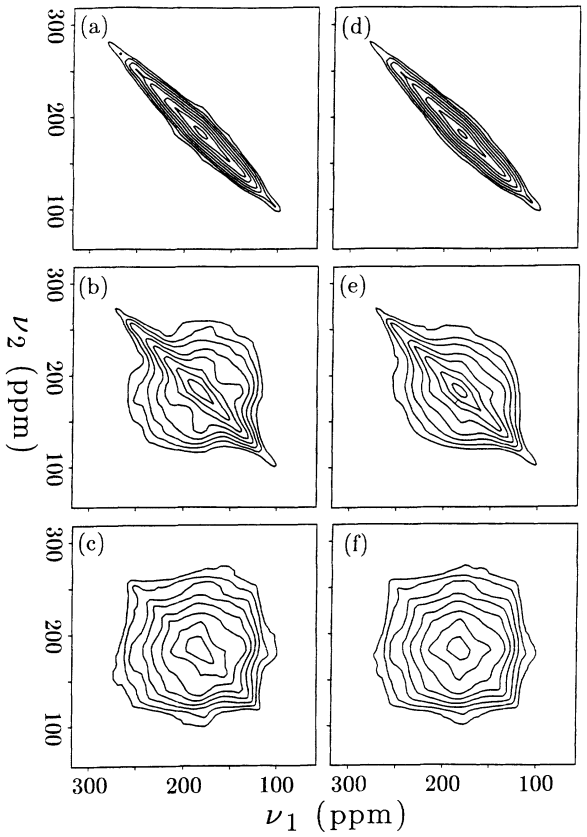

FIG. 4. Simulated 2D spectra for rotational jump models of the orientational dynamics in K_3C_{60}, at short (a),(d), intermediate (b),(e), and long (c),(f) τ_e values. (a)–(c) Model assuming complete orientational ordering and jumps by 72° about the molecular fivefold symmetry axes. (d)–(f) Model assuming $Fm\bar{3}m$ structure and jumps by 44.478° about ⟨111⟩ directions that interconnect the two inequivalent molecular orientations (see text for details of models).

structure, each C_{60}^{3-} executes jumps by the minimum-angle rotations (44.478° about four of the ⟨111⟩ directions) that interconnect the inequivalent orientations. Figures 4(d)–4(f) show simulated spectra based on this model. The diagonal ridge in Fig. 4(f) is less intense than in Fig. 4(c), due to the sixty additional accessible sites for each nucleus. The smaller jump angle also improves somewhat the resemblance to the experimental spectra at intermediate τ_e, but the evolution of the off-diagonal intensity is still better described by the isotropic rotational diffusion model. We conclude that small-angle ($<44°$) jumps must occur in K_3C_{60}. This finding implies substantial occupation of molecular orientations other than the two orientations allowed in the $Fm\bar{3}m$ structure; i.e., there is significantly more orientational disorder in K_3C_{60} than previously proposed.

Our values for A and E_a imply that the "freezing" of molecular reorientations seen at ~90 K in C_{60} [2–6] will be seen at ~166 K in K_3C_{60}. To explore possible effects of quenched disorder [5], we measured the ^{13}C T_1 after cooling the sample from 300 to 77 K at rates of ~10 K/sec and 1.25×10^{-3} K/sec. There was no cooling-rate dependence of T_1 measured either at 77 K [T_1(slow cool)=1.90±0.09 sec, T_1(fast cool)=1.82±0.09 sec] or near T_c. Since T_1 probes the electronic density of states at the Fermi surface [12,13], this result places constraints on the theoretically predicted effects of orientational disorder on the electronic properties of K_3C_{60} [8].

We thank M. J. Rosseinsky and D. W. Murphy for providing the K_3C_{60} sample.

[1] P. A. Heiney *et al.*, Phys. Rev. Lett. **66**, 2911 (1991); P. A. Heiney *et al.*, Phys. Rev. B **45**, 4544 (1992).
[2] W. I. F. David *et al.*, Nature (London) **353**, 147 (1991); W. I. F. David *et al.*, Europhys. Lett. **18**, 219 (1992); **18**, 735 (1992).
[3] R. Tycko *et al.*, Phys. Rev. Lett. **67**, 1886 (1991); R. D. Johnson *et al.*, Science **255**, 1235 (1992).
[4] X. D. Shi *et al.*, Phys. Rev. Lett. **68**, 827 (1992).
[5] R. C. Yu *et al.*, Phys. Rev. Lett. **68**, 2050 (1992).
[6] G. B. Alers *et al.*, Science **257**, 511 (1992).
[7] A. Cheng and M. L. Klein, J. Phys. Chem. **95**, 9622 (1991); M. Sprik, A. Cheng, and M. L. Klein, J. Phys. Chem. **96**, 2027 (1992); J. P. Lu, X. P. Li, and R. M. Martin, Phys. Rev. Lett. **68**, 1551 (1992).
[8] M. P. Gelfand and J. P. Lu, Phys. Rev. Lett. **68**, 1050 (1992).
[9] A. F. Hebard *et al.*, Nature (London) **350**, 600 (1991); K. Holczer *et al.*, Science **252**, 1154 (1991); R. Tycko *et al.*, Science **253**, 884 (1991).
[10] P. W. Stephens *et al.*, Nature (London) **351**, 632 (1991).
[11] J. P. McCauley *et al.*, J. Am. Chem. Soc. **113**, 8537 (1991).
[12] C. P. Slichter, *Principles of Magnetic Resonance* (Springer-Verlag, New York, 1990), 3rd ed.
[13] R. Tycko *et al.*, Phys. Rev. Lett. **68**, 1912 (1992).
[14] R. R. Ernst, G. Bodenhausen, and A. Wokaun, *Principles of Nuclear Magnetic Resonance in One and Two Dimensions* (Oxford, New York, 1987).
[15] C. Schmidt, B. Blümich, and H. W. Spiess, J. Magn. Reson. **79**, 269 (1988); B. Blümich and H. W. Spiess, Angew. Chem. Int. Ed. Engl. **27**, 1655 (1988).
[16] H. Sillescu, J. Chem. Phys. **54**, 2110 (1971).
[17] C. Christides *et al.*, Phys. Rev. B **46**, 12088 (1992).